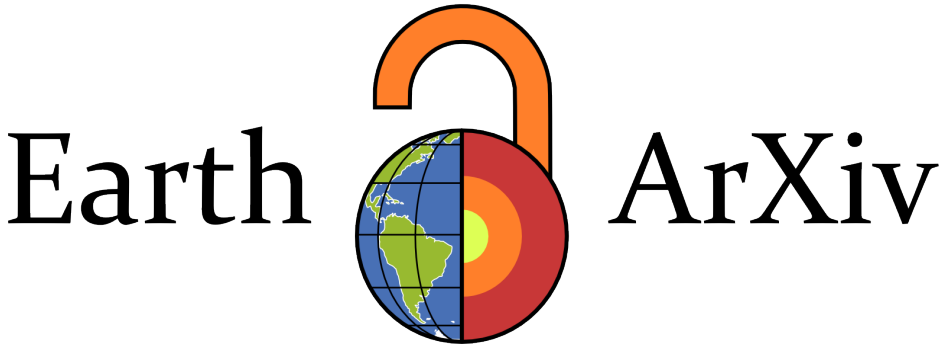

Peer review status:

This is a non-peer-reviewed preprint submitted to *Atmospheric Research* (December 2025).

Seasonal Wind Turbine-Associated Lightning in Central Europe

M. Kákona[a,b,c], R. Duspara[d], Z. Sokol[e], J. Popová[e], J. Chum[e], J. Šlegl[a,f], M. Sommer[a], M. Lužová[a,f], R. Dvořák[a], V. Hanousek[g], J. Kákona[a,h], A. Kostinsky[a], I. Ambrožová[a], O. Ploc[a]

[a]*Nuclear Physics Institute of the CAS, Husinec-Řež 130, Řež, 25068, Czech Republic*
[b]*Institute of Experimental Physics SAS, Watsonova 47, Košice, 04001, Slovakia*
[c]*Lawrence Berkeley National Laboratory, 1 Cyclotron Road, Berkeley, CA, 94720, USA*
[d]*Czech Thunderstorm Research Association, Prague, Czech Republic*
[e]*Institute of Atmospheric Physics of the CAS, Boční II 1401/1a, Prague, 14100, Czech Republic*
[f]*Faculty of Nuclear Sciences and Physical Engineering, Czech Technical University in Prague, Břehová 7, Prague, 11000, Czech Republic*
[g]*Institute of Information Theory and Automation of the CAS, Pod Vodárenskou věží 1143/4, Prague, 18200, Czech Republic*
[h]*Faculty of Electrical Engineering, Czech Technical University in Prague, Technická 2, Prague, 16627, Czech Republic*

Abstract

We report systematic evidence for a statistically distinguishable subset of cold-season lightning episodes in Central Europe that shows a distinct and recurrent association with wind turbines. Using Blitzortung stroke data from 2021 to 2024, ENTLN classifications from 2023, and local electric-field measurements, we identify episodes in which lightning activity is concentrated near wind turbines, detected cloud-to-ground strikes are consistently of negative polarity, and the cloud region passing the turbines exhibits a strongly negative electric field measured at the ground. These findings have implications both for understanding cold-season lightning processes and for assessing turbine-related lightning risk.

Keywords: Lightning, Wind turbines, Winter lightning, Blitzortung, ENTLN, Electric field mill

1. Introduction

Terminology used throughout this paper follows the definitions given in Appendix A.

Lightning strikes pose a significant hazard to wind turbines (Candela Garolera et al., 2016), particularly during winter (Montanyà et al., 2016). Japanese coastal regions document that up to 95% of turbine strikes occur in the cold season (Matsui et al., 2020), but winter lightning in connection with wind turbines in inland continental Europe remains poorly understood.

Although some studies report changes in cloud-to-ground lightning statistics following the installation of wind farms (Chen et al., 2021), including case studies showing up to 93% of winter strokes located in the vicinity of turbines in southwestern France (Soula et al., 2019), and several theories attempt to explain how wind turbines may initiate lightning discharges (Montanyà et al., 2014), the underlying mechanisms remain unresolved. Experimental data that would allow a complete understanding of the interaction between wind turbines and lightning remain limited.

Between 2018 and 2019, amateur observers from the Czech Thunderstorm Research Association noticed unusual winter lightning near wind farms in western Czechia and eastern Germany (Czech Thunderstorm Research Association, 2019, 2021). These observations raised the question whether effects similar to those reported in other regions of the world may also occur in Central Europe. Since 2021, stroke-level data from the radio lightning detection network Blitzortung (Wanke, 2011) have enabled systematic investigation of this phenomenon.

Motivated by these observations, and enabled by the recent availability of Blitzortung data, the objectives of this study are to:

1. test whether cold-season lightning strokes occur with statistically significant proximity to wind turbines in Central Europe,
2. characterize their type and, in the case of strikes, their polarity,
3. analyze local electric field conditions during the cold season.

2. Methods

We analyze lightning strokes detected by radio detection networks from 2021 to 2024 and wind turbine positions obtained from OpenStreetMap (OSM) (OpenStreetMap contributors, 2024) as available in the 2024 dataset.

2.1. Study Area and Electric Field data

The study area (Fig. 1) is defined as a circle of radius 60 km centered at (50.26°N, 12.52°E), where Boltek EFM-100 electric field mill (Boltek Corporation, 2023) (EFM) is located. According to OSM (January 2025), this area contains 369 wind turbines and 47 other high-rise structures.

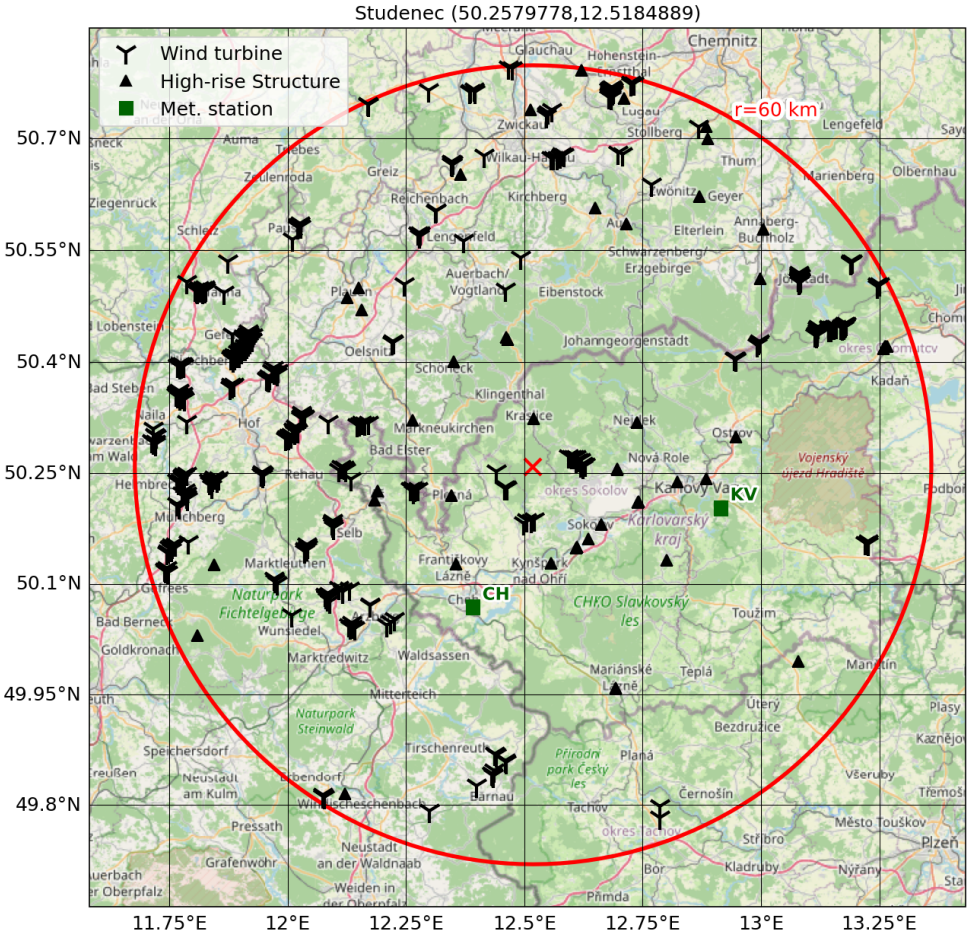

Figure 1: Map of the study area with the locations of wind turbines and high-rise structures within a 60 km radius. Map data © OpenStreetMap contributors, licensed under ODbL 1.0. The red cross mark in the center is the position of our EFM sensor. Green squares labelled CH and KV indicate the locations of the Cheb and Karlovy Vary meteorological stations, respectively.

2.2. Extraction of Lightning Strokes

Lightning strokes were obtained from two complementary radio-based detection networks: Blitzortung and ENTLN.

2.2.1. Blitzortung

The Blitzortung VLF/LF network (Wanke, 2011) locates radio sources associated with rapid changes in lightning channel current using the Time Difference of Arrival (TDoA) method. It is a community-operated system with global coverage and publicly available stroke-level data. Blitzortung does not provide stroke classification (IC vs. CG; please see Appendix A for terminology) or polarity information; it reports only the estimated source location and timestamp of each detected electromagnetic impulse. Blitzortung data were used for the full analysis period 2021–2024.

2.2.2. ENTLN

The Earth Networks Total Lightning Network (Zhu et al., 2017, 2022) provides stroke classification (IC vs. CG), altitude, and in the case of CG strikes (reported altitude of zero) strike polarity (CG−/CG+; please see Appendix A for terminology). A classification confidence threshold of $\geq$80% was applied throughout to eliminate borderline cases. Following the reported upgrade of the ENTLN network (Zhu et al., 2022), only data from 2023 onward were considered sufficiently spatially consistent over Europe. ENTLN data were therefore used exclusively for case studies from 2023 onward.

2.2.3. Location accuracy in the study region

The horizontal location accuracy of Blitzortung has been reported as approximately 1.4 km (Narita et al., 2018), based on measurements conducted in Japan. To verify whether this value is representative for the Central European domain studied here, we performed a cross-comparison against ENTLN CG strikes recorded on 15 August 2023 during an extensive thunderstorm, within a time window of $\pm$100 ms.

Of the 892 qualifying ENTLN CG strikes and 5,957 Blitzortung strokes recorded on that day in the study region, 86 pairs were successfully matched. The low pairing fraction reflects the different detection philosophies of the two networks: whereas ENTLN CG strikes (confidence $\geq$80%) represent a filtered subset of ground-reaching discharges, Blitzortung reports all detected electromagnetic impulses regardless of discharge type, the majority of which are intracloud strokes without a corresponding CG counterpart. For the

matched pairs, the median spatial separation between ENTLN and Blitzortung was 1.43 km. The median absolute time difference was 3 μs, confirming strong temporal agreement. The systematic spatial bias was: 1.29 km in the latitudinal and -0.62 km in the longitudinal direction.

These results confirm that the 1.4 km location accuracy reported by Narita et al. (2018) is representative also for the Central European domain studied here, and provide a regional empirical basis for the 1.4 km threshold used throughout this study.

2.3. Extraction of Wind Turbines and High-Rise Structures

Geographical positions of wind turbines and high-rise man-made structures were extracted from OpenStreetMap (OSM) using the Overpass Turbo API (Overpass API Developers, 2025). OSM data quality in Europe is more than adequate for this purpose, with typical horizontal accuracy on the order of 1.5 m (Haklay, 2010), which is negligible compared to the uncertainty of lightning location.

Wind turbine coordinates were obtained using the query given in Appendix B.1. High-rise structures other than wind turbines were obtained using the query given in Appendix B.2.

High-rise structures, in our study, are defined as man-made objects with a height exceeding 70 m above ground level or buildings with more than 25 floors. This includes skyscrapers, communication towers and masts, tall chimneys, cooling towers, and similar structures.

2.4. Radar data

Radar data were acquired by a Doppler dual-polarisation C-band radar operated by the Czech Hydrometeorological Institute (CHMI), located at the Praha peak (862 m a.s.l.) in the Brdy Hills (49.66°N, 13.78°E). The distance from the radar to the EFM site is approximately 110 km, and the distances to the wind turbines in the study area range from approximately 100 to 120 km.

For radar analysis, we used the **MAX3D** product, which represents the **maximum reflectivity in a vertical column** above each grid point. During the documented episodes, this composite reflectivity captured echo maxima located at altitudes of approximately **2–4 km** above mean sea level. The spatial resolution of the MAX3D radar field is 1 km $\times$ 1 km per pixel. MAX3D was used to track the motion of precipitating regions relative to the EFM site and the wind turbines.

In addition to MAX3D, we used the CAPPI 2 km radar product (Constant Altitude Plan Position Indicator at 2 km) to analyse precipitation intensity and the horizontal structure of radar reflectivity.

2.5. Reanalysis-based meteorological classification

ERA5 reanalysis data (Hersbach et al., 2020) were used to classify the large-scale meteorological environment. Because of the relatively coarse spatial and temporal resolution of the dataset, an analysis at the exact location and time of the event was not feasible. Instead, a 5×5 grid of nodes encompassing the central part of the study area was examined in order to characterize the environmental conditions within the region of interest.

The classification was based on near-surface temperature and relative humidity, the vertical extent of saturated layers, and the heights of the 0°C, −10°C and −20°C isotherms. In addition, conditions relevant to thunderstorm electrification were assessed. Following Stucke et al. (2024), the presence of liquid water near the −10°C level was used as an indicator of environments favourable for non-inductive charging processes.

2.6. Distance Computation

Distances between each Blitzortung stroke and the nearest wind turbine or high-rise structure were computed using great-circle distances.

3. Results

3.1. Stroke distribution relative to ground objects

Because the spatial distribution of wind turbines and high-rise structures is inherently uneven, it is first necessary to characterise their statistical distribution across the landscape. To this end, we generated a synthetic dataset of 1000 strokes with a uniform spatial distribution and constructed the corresponding histogram (Fig. 2). This reference distribution provides a baseline that allows a meaningful comparison with the probability distribution of lightning events, both those unrelated to wind turbines and those observed during real lightning episodes.

An identical distance-to-object analysis applied to the real strokes from the 24 November 2023 snowstorm (Fig. 3), shows that more than 94.5% of the strokes occurred within 1.4 km of a wind turbine, whereas none were located within this distance of high-rise structures. Let us recall that a distance of 1.4 km corresponds to the reported location accuracy of the Blitzortung

network. This episode is presented solely as an illustrative example intended to demonstrate the shift in the statistical distribution of strokes. It was selected because it generated lightning strokes throughout the full spatial extent of the study area.

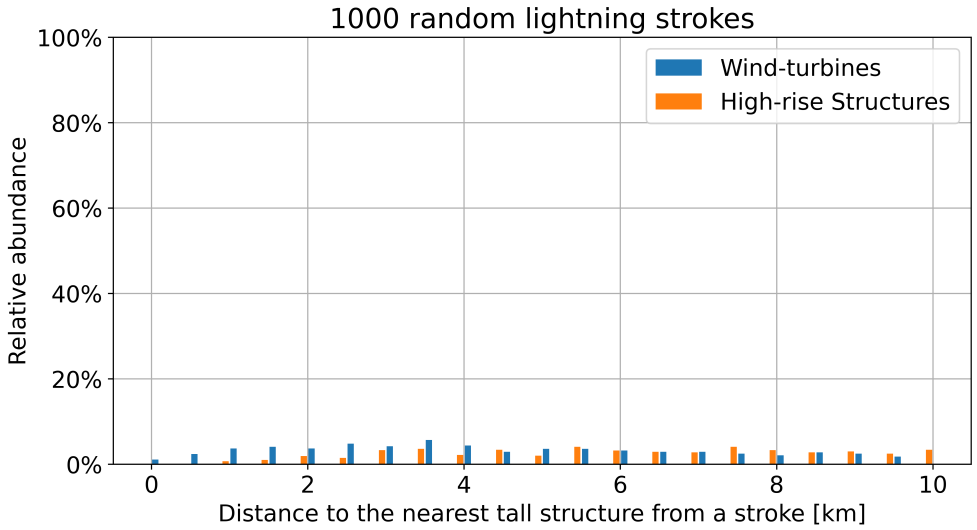

Figure 2: Histogram of distances to the nearest wind turbine (blue) and high-rise structure (orange) for 1000 randomly generated strokes within the study area.

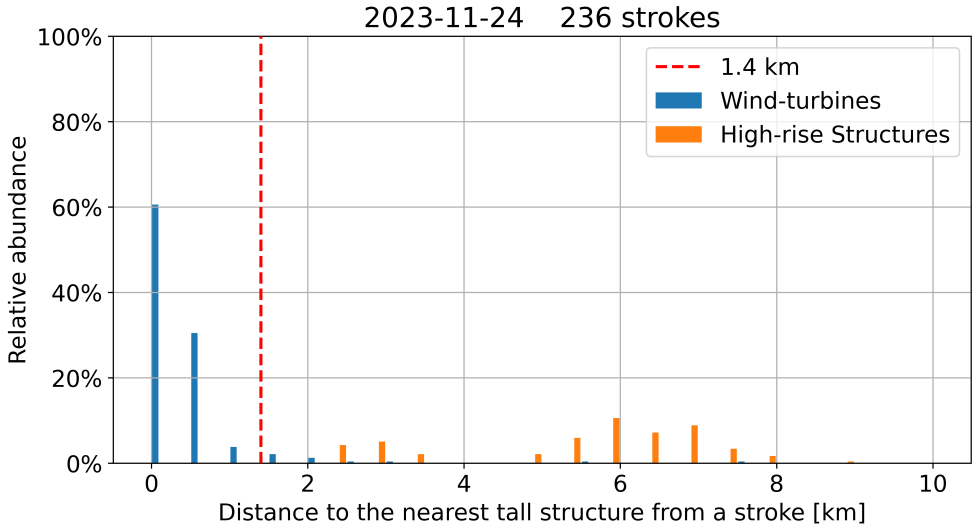

Figure 3: Histogram of distances to the nearest wind turbine (blue) and high-rise structure (orange) for 236 lightning strokes detected during the 24 November 2023 snowstorm. A total of 94.5% of all strokes (223 out of 236) occurred within 1.4 km of at least one wind turbine. None occurred within this distance of any other high-rise structure. The dashed line marks the estimated horizontal location uncertainty (≈1.4 km).

3.2. Temporal analysis

Fig. 4 shows days (lightning episodes) with at least one stroke. Circles' sizes correspond to stroke counts during one day; vertical position is the median distance to the nearest wind turbine. The median was chosen as a single representative metric for each episode because the stroke distance distributions are typically highly skewed (Fig. 3): a small number of distant strokes would bias the mean upward, while the median robustly reflects the dominant clustering behaviour.

Table 1: Cold season (November–March) Lightning Episodes in 2023 (Date). The table lists total ENTLN Strokes (Strokes), Strokes classified with given confidence ($\geq$ 80%), Intracloud Strokes (IC), negative Strikes (CG-), positive Strikes (CG+), median Blitzortung stroke distance to the nearest wind turbine in km (Median), and weather description (observer's precipitation classification / near-ground temperature) from the Karlovy Vary meteorological station (606 m a.s.l.).

Date	Strokes	$\geq$ 80%	IC	CG-	CG+	Median [km]	Weather description
2023-01-13	8	5	0	5	0	0.3	Rain / +5 °C
2023-02-01*	35	8	1	7	0	0.7	Rain & Snow / 0 °C
2023-03-14	21	5	0	5	0	0.8	Rain / +7 °C
2023-03-25*	44	16	3	13	0	0.5	Rain / +7 °C
2023-03-30	193	124	87	35	2	13.9	Rain & Snow / +11 °C
2023-11-24*	79	37	1	36	0	0.4	Snow / +2 °C
2023-12-21	135	55	2	51	2	5.8	Rain & Snow / +6 °C

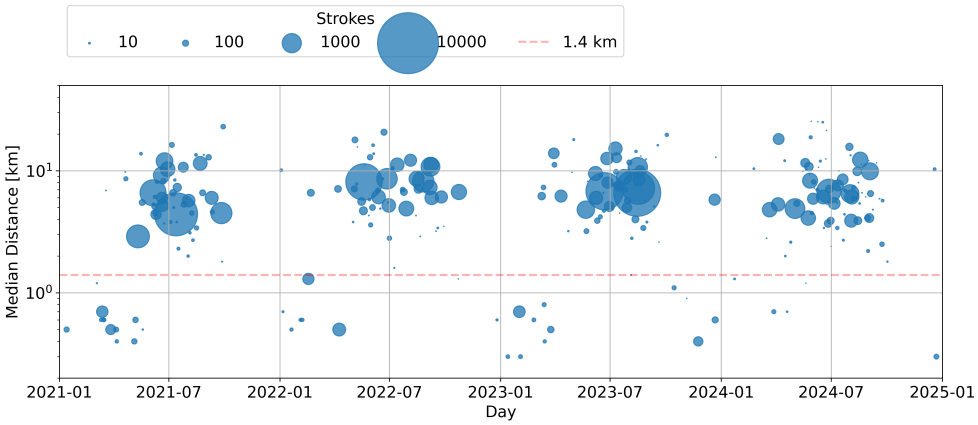

Figure 4: Daily distribution of lightning activity from winter 2021 to winter 2024. Each circle corresponds to a day with at least one detected stroke; circle diameter is proportional to stroke count. The vertical position represents the median distance to the nearest wind turbine. The dashed red line marks the estimated Blitzortung location uncertainty ($\approx$1.4 km).

3.3. ENTLN lightning classification

Tab. 1 summarises the ENTLN stroke and strike classification for cold-season (November–March) Lightning Episodes detected in the study area in 2023.

3.4. Electric field and radar data

Episodes marked with an asterisk in Tab. 1 correspond to likely strikes to wind turbines within 8 km of our EFM. Radar data (MAX3D; see Methods) were used to determine whether the same reflectivity segment passed over both the EFM and the wind turbine. Only two episodes (2023-02-01 and 2023-11-24) met this condition.

For these two episodes, we produced animations (Video 1 and Video 2) showing the evolution of the electric field (left panel) together with the corresponding radar frame (right panel). The yellow shaded region indicates the uncertainty window of the radar timestamp, because each radar image is composed of scans acquired over a period of five minutes. Axes in the radar frames indicate horizontal coordinates in kilometres. The black line outlines the border of the Czech Republic. Red dots in the electric field plot represent the distance of lightning strokes reported by Blitzortung as seen from the EFM site. The position of the EFM itself is marked by a square symbol labelled S in the radar frames. Points labelled CH and KV denote the locations of the meteorological stations Cheb and Karlovy Vary, respectively. Plus signs indicate the positions of lightning strokes, and asterisks mark the locations of wind turbines. Strokes that occur in the vicinity of a wind turbine are highlighted in red. Radar colour shading corresponds to reflectivity in dBZ.

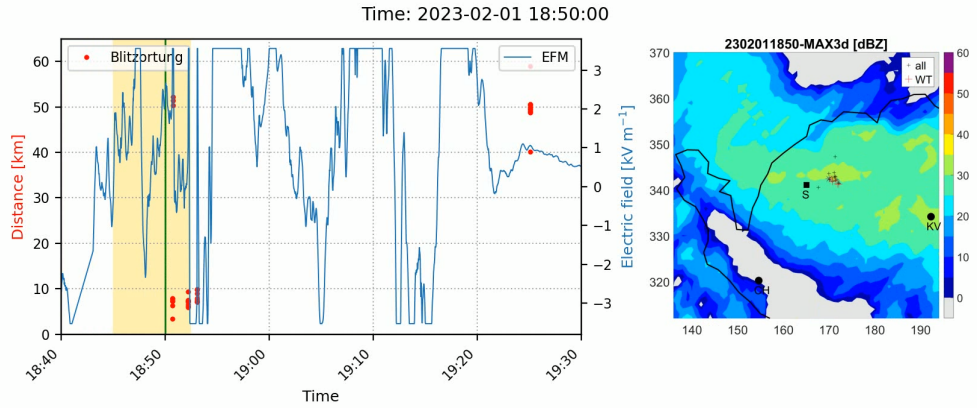

Video 1: EFM and radar data for lightning episode 1 February 2023. Animation is available here: https://youtu.be/28ao707ifls.

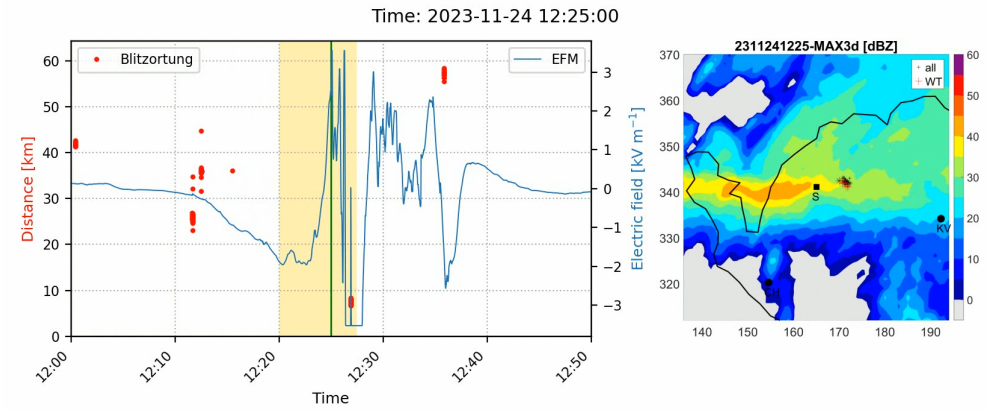

Video 2: EFM and radar data for lightning episode 24 November 2023. Animation is available here: https://youtu.be/DI3buov8Psg.

In both cases, the strike occurred when a region of 35–40 dBZ reflectivity passed over the wind turbine. According to EFM measurements, when such a region passed over the EFM location, the measured field was strongly negative. The absolute magnitude is unknown because the EFM range was set for summer thunderstorms, which rarely exhibit such strong ground-level electric fields.

During the documented cold-season lightning episodes, radar echo maxima were located at altitudes of approximately 2–4 km a.s.l. Bright-band contamination was not a concern in these cases: near-surface temperatures were close to 0°C, placing the melting layer at approximately 800 m a.s.l., well below the lowest radar beam, which samples at approximately 1600 m a.s.l. at the distances relevant to this study.

3.5. Hydrometeors classification

To characterise the microphysical composition of the precipitating cloud during the documented episodes, we analysed data from the dual-polarisation radar using the HClass hydrometeor classification algorithm (Vaisala, 2024). Vertical cross-sections oriented west–east and passing through the centre of the study area were extracted for the hour during which lightning activity was recorded.

The results for both episodes (2023-02-01 and 2023-11-24) are shown in Fig. 5 and 6. The hydrometeor distribution is consistent across both cases and corresponds to cold-season precipitation at low altitudes.

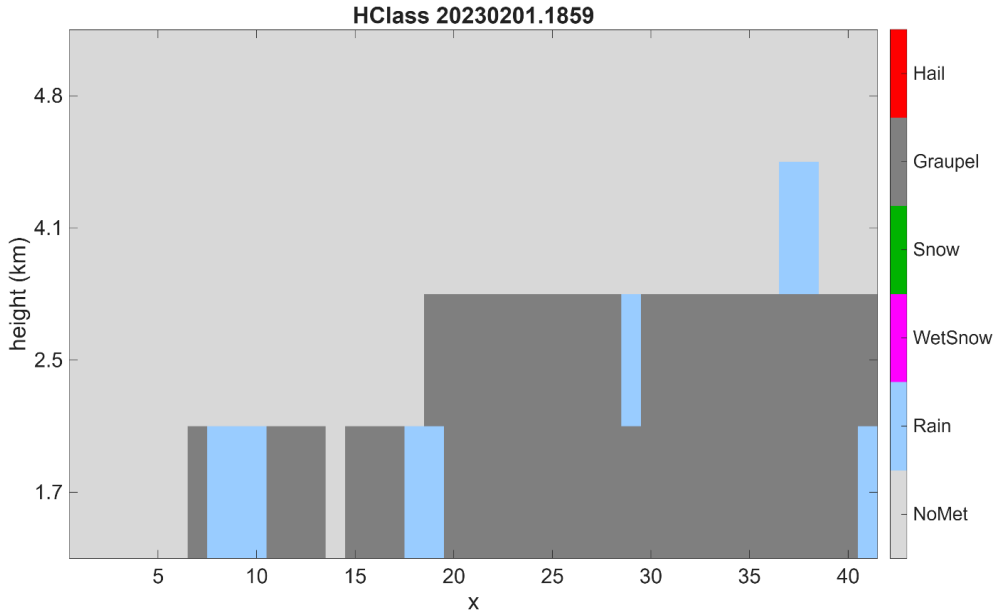

Figure 5: Hydrometeor classification (HClass) from the dual-polarisation radar for the lightning episode on 1 February 2023 (18:59 UTC). West–east vertical cross-section passing through the centre of the study area. The horizontal axis shows distance in km along the cross-section; the vertical axis shows height above mean sea level.

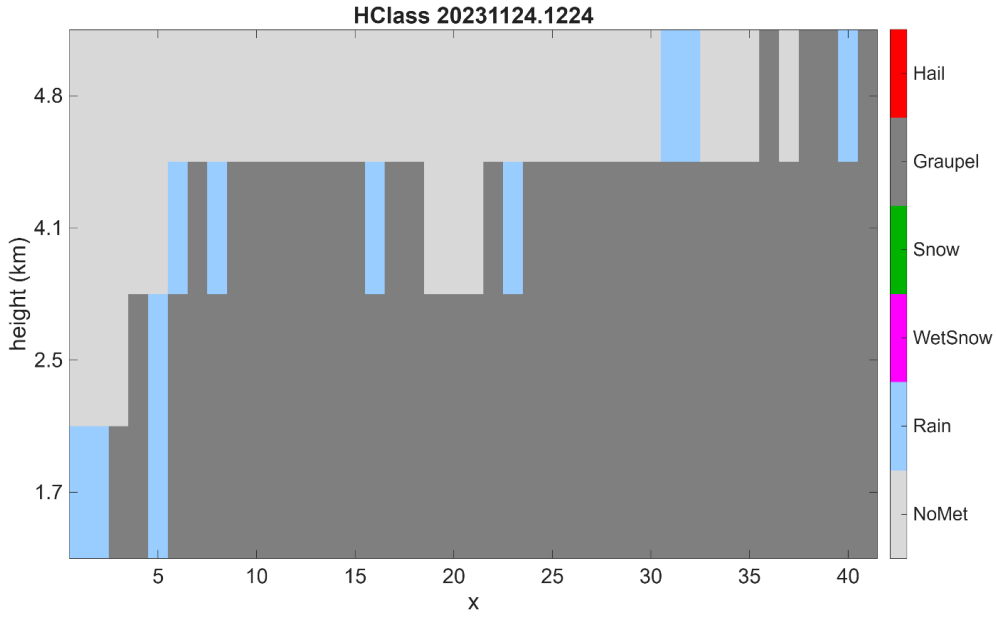

Figure 6: Hydrometeor classification (HClass) from the dual-polarisation radar for the lightning episode on 24 November 2023 (12:24 UTC). West–east vertical cross-section passing through the centre of the study area. The horizontal axis shows distance in km along the cross-section; the vertical axis shows height above mean sea level.

3.6. Meteorological characterisation of the documented episodes

Tab. 2 summarises the meteorological parameters derived from ERA5 for the two case-study episodes (2023-02-01 and 2023-11-24).

Near-surface temperatures and relative humidity were consistent with observations from the Karlovy Vary and Cheb meteorological stations, and homogeneous cloud cover was independently confirmed by radar data and visibility observations at both stations.

Table 2: Meteorological parameters derived from ERA5 reanalysis for the two case-study episodes.

Parameter	2023-02-01	2023-
2-m air temperature (°C)	−1 to +1	−1 to
Relative humidity (%)	∼100	∼1
Layer with RH ≈ 100%	Surface to ∼4 km	Surface to
Height of melting layer / 0°C isotherm (km a.s.l.)	∼0.8	∼0
Height of −10°C isotherm (km a.s.l.)	2.2	2.
Height of −20°C isotherm (km a.s.l.)	3.6	3.
Liquid water near −10°C level	>50% of grid points	>50% of g
Environment type	Wind-field thunderstorm	Wind-field th
Dominant forcing mechanism	Large-scale dynamical	Large-scale
Layer favourable for non-inductive charging (km a.s.l.)	∼0.8–2.2	∼0.8

3.7. Electric field comparison: winter vs. summer

Another noteworthy result is that the electric fields generated by winter clouds often reach higher magnitudes than those observed during most summer storms.

For comparison, we include typical EFM records of a winter lightning episode (Fig. 7) and a summer thunderstorm (Fig. 8), both recorded with the same instrument at the same location. Both episodes produced lightning events within 8 km of the instrument, and the record duration and vertical scaling are identical. The markedly higher electric field magnitudes observed in the winter case are consistent with a low cloud base placing the main negative charge region in closer proximity to the surface.

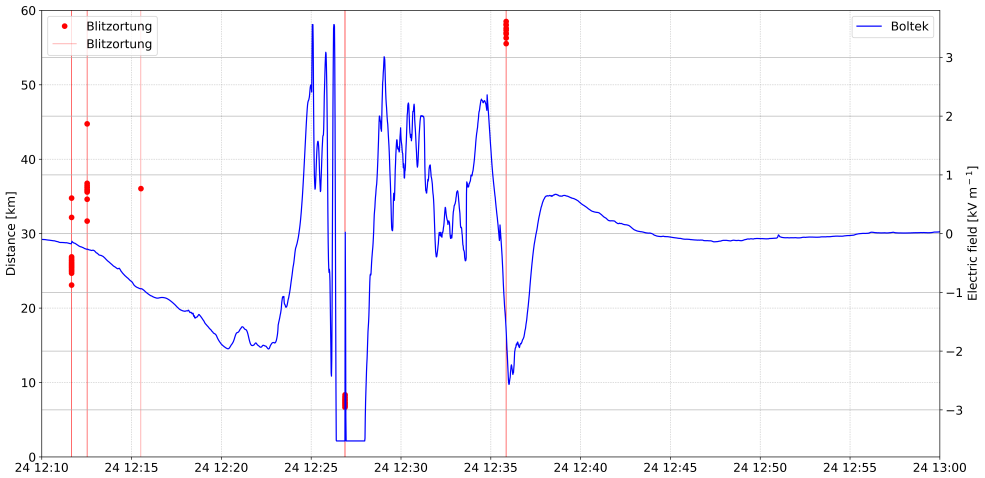

Figure 7: Electric field record during the lightning episode on 24 November 2023. Distances of the detected strokes (red dots) are given relative to the location of the EFM instrument. Note that the electric field record is out of range around the time of the closest discharge.

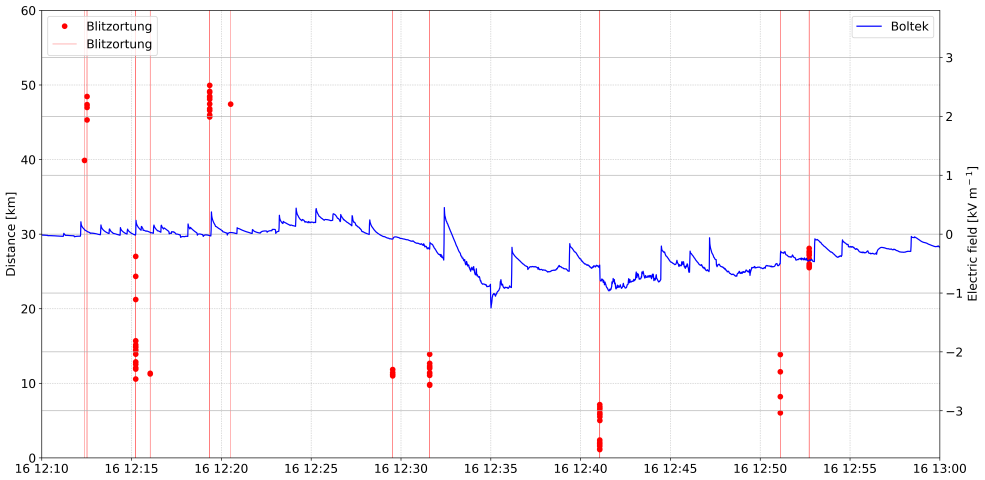

Figure 8: Electric field record during the lightning episode on 16 August 2023. Distances of the detected strokes (red dots) are given relative to the location of the EFM instrument.

3.8. Case study: lightning episode with exclusive wind turbine association

We present an example of a lightning episode that produced wind turbine-associated lightning events only. Grouping all strokes occurring within one second (twice the median lightning-event duration reported by Kákona et al.

(2023)) into a single lightning event, we constructed the animation (Video 3) in which each event is visualised by cyan circles marking its constituent strokes. If any stroke within an event falls closer than 1.4 km to a wind turbine, that turbine is highlighted with a red dot.

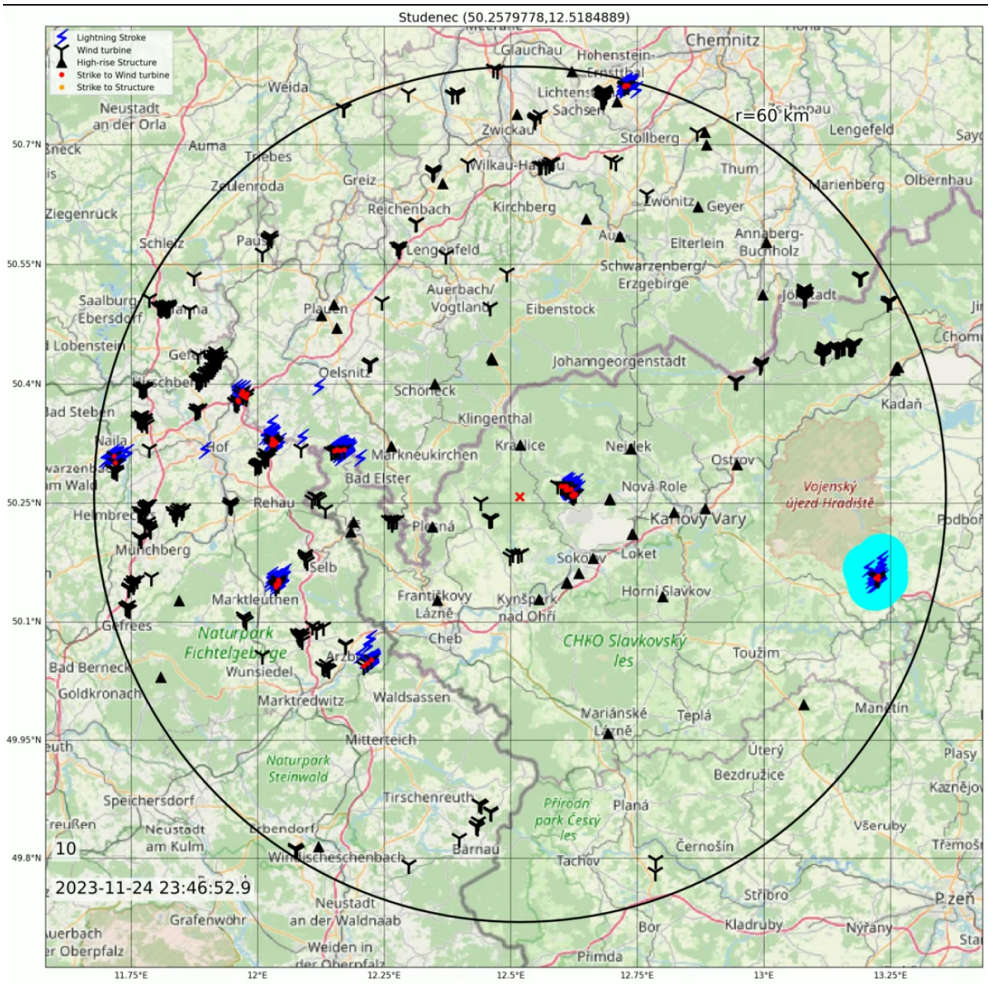

Video 3: Animation of the lightning episode on 24 November 2023. Animation is available at: https://www.youtube.com/watch?v=jIgVS3HVkIo.

4. Discussion

The histogram of stroke distances relative to ground structures (Fig. 3) indicates a clear dependence on the positions of wind turbines during the

selected real lightning episode. To examine the seasonal behaviour of this pattern, we constructed Fig. 4. To distinguish individual episodes, we calculated the median distance between each stroke and the nearest wind turbine. This metric is particularly important because a lightning event may extend over a large area, and only a subset of its detected strokes may actually approach a turbine. It must also be emphasised that the Blitzortung network does not provide information on whether a given stroke is a strike. In the plots, the red dashed line marks the 1.4 km threshold, which we adopt as the approximate location accuracy of the Blitzortung system.

The figure shows that episodes with strokes near wind turbines occur predominantly during the cold season (November–March). We therefore refer to this pattern as **Seasonal Wind Turbine-Associated Lightning (SWAL)**.

One might argue that the observed spatial association between cold-season lightning and wind turbines is not a novel finding, since winter lightning to tall man-made structures is well documented (Azadifar et al., 2016; Heidler et al., 2013; Smorgonskiy et al., 2013, 2015; Stucke et al., 2024; Morgenstern et al., 2022), and the probability of a lightning strike is known to increase with object height (Eriksson, 1987; Rakov, 2003). However, wind turbines differ from static tall structures in several aspects relevant to lightning initiation. Rotating blade tips avoid the accumulation of self-produced space charge and are therefore exposed to stronger local electric fields than static objects of comparable height (Montanyà et al., 2014). Furthermore, the composite materials of wind turbine blades are susceptible to triboelectric charging through collisions with hydrometeors such as snow and ice particles, a mechanism analogous to the electrostatic charging documented for helicopter rotor blades operating in snowy conditions (Grosshans et al., 2017). These properties suggest that wind turbines may trigger lightning under meteorological conditions distinct from those associated with upward lightning from static towers.

The study area contains both wind turbines and 47 other high-rise structures of comparable or greater height. The reference distribution of randomly placed strokes (Fig. 2) establishes the expected stroke-to-object association under the null hypothesis of no preferential attraction. During SWAL episodes, the stroke distribution observed for wind turbines deviates significantly from the reference distribution, whereas no comparable deviation is found for tall static structures. Fig. 3 shows a representative example of this pattern for the 24 November 2023 episode; the similar contrast between

wind turbines and tall static structures is observed consistently across all episodes with a median stroke–turbine distance smaller than 1.4 km. Since both object types are present within the same spatial domain and are subject to identical meteorological conditions during each episode, this contrast cannot be attributed to differences in object density or spatial coverage. It should be noted, however, that the study area contains only nine structures exceeding 150 m in height, excluding wind turbines. The absence of observed strikes to these structures during SWAL episodes is therefore of limited statistical significance and cannot be used to conclude that tall static structures are categorically unaffected. We therefore hypothesise that wind turbines represent a distinct category of lightning-attracting structures under SWAL conditions, and that direct comparison with the tower lightning literature is not straightforward.

On the basis that wind turbines represent a structurally distinct category of lightning-attracting objects, we now turn to the meteorological conditions under which SWAL episodes occur. ERA5 reanalysis data show that near-surface temperatures during both case study episodes were close to 0°C, relative humidity was near 100% from the surface up to approximately 4 km, and the −10°C and −20°C isotherms were located at approximately 2.2 and 3.5 km, respectively. These conditions are characteristic of the wind-field thunderstorm subtype (Morgenstern et al., 2022). Wind-field thunderstorms are characterised by shallow clouds with a large fraction of the cloud layer warmer than −10°C and driven by large-scale dynamical forcing rather than convective instability (Morgenstern et al., 2022). According to the classification criterion of Stucke et al. (2024), the presence of liquid cloud water at the −10°C isotherm level is a defining characteristic of this subtype; more than half of the considered ERA5 grid points satisfied this condition at the nearest available pressure levels for both episodes. It should be noted that wind-field thunderstorms do not account for all cold-season lightning activity in the study region, as illustrated by the episodes on 2023-03-30 and 2023-12-21 in Tab. 1, which exhibit median stroke–turbine distances well above 1.4 km and are therefore not classified as SWAL.

The cloud electrification conditions during SWAL episodes differ markedly from winter lightning observations in Japan, where lightning to wind turbines is predominantly of positive or bipolar polarity and is typically initiated by upward leaders (Matsui et al., 2020), associated with the tilted-dipole charge structure characteristic of Japanese coastal winter thunderstorms (Brook et al., 1982). In contrast, ENTLN data show that in SWAL episodes, the

detected strikes were consistently of negative polarity, suggesting a different charge structure. This is independently supported by EFM measurements: for both case study episodes, a strongly negative electric field was recorded at the EFM site when the radar reflectivity segment that had been located above the wind turbine at the time of the strike subsequently passed over the EFM location.

The ERA5 reanalysis data show that the -10°C isotherm was located at approximately 2.2 km and the melting layer at approximately 0.8 km a.s.l., placing the entire temperature range relevant to non-inductive charging between these altitudes (Takahashi, 1978; Saunders et al., 2006). The HClass hydrometeor classification (Fig. 5 and 6) confirms the presence of graupel throughout this zone, satisfying the microphysical conditions necessary for non-inductive charge separation (Takahashi, 1978). These observations indicate that cloud electrification did occur during the documented episodes, and that both the main negative charge layer and a lower positive charge layer are expected.

The EFM records for both case study episodes show repeated sign reversals of the electric potential gradient during the passage of the precipitation system (Video 1 and Video 2). This pattern is consistent with a succession of precipitation bands (Takahashi et al., 1999), each with a distinct spatial charge structure, passing over the EFM site (Fig. 9).

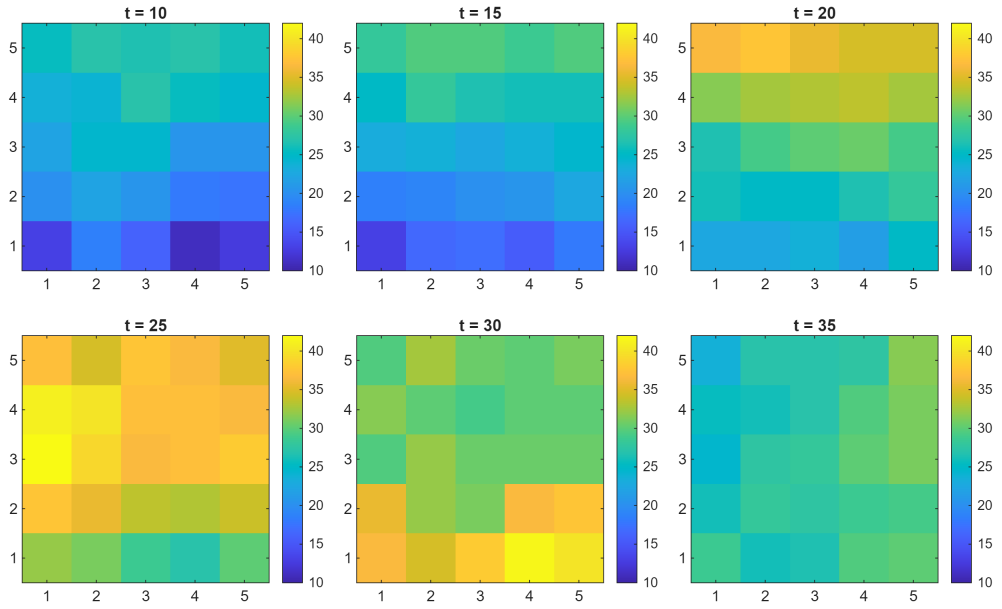

Figure 9: Time evolution of radar reflectivity (CAPPI at 2 km altitude) during the lightning episode on 24 November 2023. The horizontal axis shows time in minutes elapsed since 12:00 UTC, corresponding to the start of each radar scan. Reflectivity is colour-coded in dBZ. The field covers a 5 × 5 km area with 1 km × 1 km pixel resolution; the EFM site is located at the central pixel. The figure demonstrates that precipitation intensity varies in time and is inhomogeneous in the horizontal plane, supporting the hypothesis of a succession of precipitation bands. A pronounced inhomogeneity is evident in the interval 25–30 min, coinciding with the strongly negative electric potential gradient recorded by the EFM (Video 2 and Fig. 7).

We speculate that two complementary mechanisms may contribute to the preferential association of SWAL discharges with wind turbines. First, in precipitation bands where the lower positive charge layer is locally absent or weakly developed, the main negative charge region is directly exposed above the ground objects. Second, collisions of positively charged precipitated hydrometeors with the non-conductive blade surfaces may charge the blades positively (Grosshans et al., 2017), a process that is particularly effective for rotating blades (Montanyà et al., 2014). Both mechanisms are illustrated schematically in Video 4.

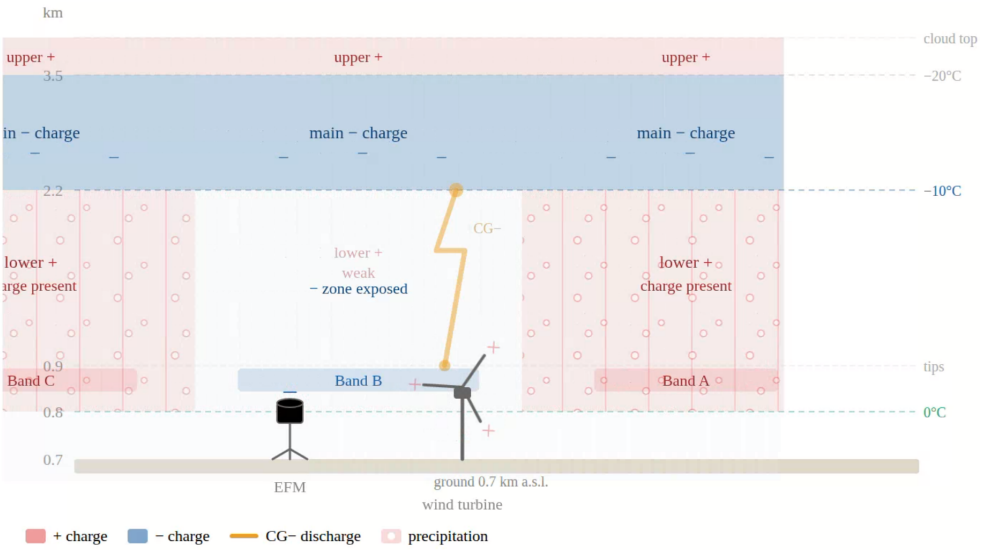

Video 4: Schematic animation of the proposed SWAL discharge mechanism. A succession of precipitation bands passes over the wind turbine from left to right. In Band A, positively charged hydrometeors triboelectrically charge the rotating blades. In Band B, where the lower positive charge layer is weak or absent, the main negative charge region is directly exposed above the turbine, providing favourable conditions for a negative cloud-to-ground discharge. The electric field mill (EFM) records the corresponding sign reversals of the electric potential gradient. Animation available at: https://youtu.be/rytdPtL3PAQ.

It should be noted that direct electric field measurements in the immediate vicinity of wind turbines are not available in this study, and that the turbine structure itself is expected to significantly distort the local electric field (Montanyà et al., 2014). The proposed mechanisms therefore remain speculative and should be tested by dedicated field campaigns.

Because the documented episodes produce strikes only in the vicinity of wind turbines and do not resemble fully developed thunderstorms capable of producing lightning to ground-level objects such as trees or low-rise buildings, it remains uncertain whether the observed meteorological conditions would have evolved into a typical winter storm in the absence of wind turbines. The term SWAL is therefore descriptive and does not imply a conventional winter lightning regime.

5. Conclusion

This study provides systematic evidence that a subset of cold-season lightning in Central Europe forms a distinct and recurrent pattern associated with wind turbines. Analysis of four years of Blitzortung stroke data, supported by ENTLN classification and local electric field measurements, reveals a statistically distinguishable subset of cold-season lightning episodes. We refer to this pattern as **Seasonal Wind Turbine-Associated Lightning (SWAL)**.

Episodes classified as SWAL are characterised by three consistent observational features: (i) their strokes occur in proximity of wind turbines, (ii) the strikes are consistently of negative polarity, and (iii) the cloud region passing the wind turbines exhibits a strongly negative electric field measured at the ground.

These findings raise an important question: **Would SWAL-like episodes occur even without wind turbines, or do turbines modify the local electric environment in a way that enables lightning that would not otherwise develop?**

The results presented here highlight the need for high-resolution modelling and targeted observations of cold-season cloud electrification in the vicinity of large wind farms. Understanding whether SWAL is a turbine-induced process, or a naturally occurring but previously unrecognized mode of winter lightning, will be essential both for lightning physics and for the assessment of turbine-related lightning risk in Central Europe.

The identification of SWAL as a statistically distinguishable subset of cold-season episodes, characterised by a strong spatial association with wind turbines and consistently negative polarity, offers a rare opportunity to study the boundary conditions under which negative cloud-to-ground discharges develop, a question of broader relevance to lightning physics and to our understanding of cloud electrification processes.

We encourage the lightning research community to investigate SWAL-like episodes using additional lightning detection networks and measuring apparatuses in order to assess whether similar patterns can be identified independently.

Acknowledgements

This work was supported by the EU Operational Programme *Research, Development and Education* (OP RDE) under the project **CRREAT – Re-**

search Centre of Cosmic Rays and Radiation Events in the Atmosphere. The lead author, M. Kákona, was supported by the **Fulbright–Masaryk Fellowship**.

This research was also supported by the Johannes Amos Comenius Programme (OP JAK) under project no. CZ.02.01.01/00/22_008/0004605 "Natural and anthropogenic georisks".

The authors gratefully acknowledge **Egon Wanke** and **Günther Reitz** for his assistance in obtaining stroke data from the Blitzortung.org lightning detection network, and the volunteers and station operators of the **Blitzortung.org** lightning detection network for providing community accessible stroke data that made this analysis possible.

We also thank the **Earth Networks Total Lightning Network (ENTLN)** for supplying lightning classification and polarity information used in this study.

We sincerely acknowledge the global **OpenStreetMap community** for their continuous volunteer contributions that enable open, high-quality geospatial datasets. Wind turbine and infrastructure data used in this work were obtained from OpenStreetMap and are © OpenStreetMap contributors, distributed under the **Open Database License (ODbL) 1.0**.

We also acknowledge the **Czech Hydrometeorological Institute (CHMI)** for providing access to radar and meteorological data, including the MAX3D reflectivity product used in this study.

The authors acknowledge the **EURADOS Working Group 11** (High Energy Radiation Fields) for establishing the collaborative platform under which the participating institutions contributed their expert knowledge to this study.

Appendix A. Terminology and Definitions

Lightning science spans multiple measurement domains (optical, radio, electrostatic, current sensing,...), each using partly overlapping terminology. Commonly used terms such as *flash*, *stroke*, *strike*, or *lightning* do not necessarily refer to the same physical phenomenon. To ensure clarity and reproducibility, we explicitly define the terminology adopted in this study. Definitions follow the operational criteria used in our analysis and may differ from conventions used in other subfields.

Appendix A.1. Lightning Stroke

The lightning channel current can be written as

$$I(t) = I_{\text{slow}}(t) + I_{\text{fast}}(t),$$

where the slow component represents quasi-steady current and the fast component represents rapid impulsive changes (e.g., return strokes, recoil leaders).

Loop antennas used in lightning detection systems do not measure the current directly. A voltage (electromotive force, EMF) is induced at the antenna terminals according to Faraday's law in response to the time derivative of the magnetic field produced by the lightning channel. The induced EMF $\mathcal{E}(t)$ may be approximated as

$$\mathcal{E}(t) = -M_{\text{eff}} \frac{dI_{\text{fast}}}{dt},$$

where M_{eff} is the effective mutual inductance between the lightning channel and the antenna. This mutual inductance depends on the distance and relative orientation between the channel and the loop, on the geometry of the current path, and on the frequency-dependent response of both the antenna and the front-end electronics.

Because $I_{\text{slow}}(t)$ varies only on time scales much longer than the antenna bandwidth, its contribution to dI/dt and therefore to the induced EMF is negligible. The measured voltage predominantly reflects the fast impulsive component of the lightning current, and provides a distorted band-limited estimate of dI_{fast}/dt.

For the purposes of this study, we define a *Lightning Stroke* as any detected EMF peak, irrespective of whether it corresponds to a return stroke, recoil leader, or another fast impulsive process during a lightning.

Appendix A.2. Lightning Event or simple Event

A Lightning Event represents the full electromagnetic activity associated with a lightning phenomenon over a short interval of time. In this study, a Lightning Event is defined as a contiguous sequence of lightning strokes with a total duration of up to 1 s. This threshold is motivated by the median lightning-event duration of approximately 0.5 s reported in Kákona et al. (2023). Rare cases of substantially longer events may occur, but their frequency is sufficiently low that they do not affect the statistical conclusions of this work.

Because a term with a similar meaning, flash, is typically used in optical detection systems, we avoid that terminology and use Lightning Event consistently for radio-derived temporal clusters of strokes.

Appendix A.3. Lightning Episode

In this study, we use the term *Lightning Episode* to describe a meteorological situation that might traditionally be referred to as a "thunderstorm". Because our analysis focuses on the cold season, we avoid presuming that such episodes exhibit the characteristics of summertime-like thunderstorms.

A Lightning Episode is therefore defined as a cluster of Lightning Events that were radio-detected within the study area, typically occurring within a single calendar day. This terminology captures the meteorological context of winter lightning without implying the presence of a fully developed thunderstorm.

Appendix A.4. Lightning Strike

A stroke classified by the lightning detection network as a cloud-to-ground (CG) lightning discharge is labeled as a *Strike*. A single Lightning Event may contain multiple strikes. In this study, we do not distinguish between downward and upward strikes, as such discrimination is beyond the resolution and capability of the detection systems used.

Appendix A.5. Strikes/Strokes Polarity

If a lightning discharge does not reach the ground, it is classified as an intracloud stroke (IC). For IC strokes, the concept of polarity is not defined, as the discharge develops between regions of opposite charge within the cloud and does not provide a unique reference for charge transfer.

For strokes reaching the ground (hereafter referred to as strikes), polarity is defined according to the convention introduced by (Rakov and Uman, 2003). A negative cloud-to-ground (CG−) strike transfers negative charge from the cloud to the ground, while a positive cloud-to-ground (CG+) strike transfers positive charge to the ground.

Strikes can be further classified as downward or upward, depending on the direction in which the dominant part of the lightning channel develops. The polarity of upward strikes is defined in the same way as for downward strikes, i.e. according to the sign of the charge transferred to the ground, regardless of the direction of channel development.

Consequently, upward lightning with a dominant (longer) positive channel is classified as CG−, analogously to downward lightning with a dominant (longer) negative channel, since in both cases the direction of current flow is the same and negative charge is transferred to the ground.

Appendix A.6. Limitations of Stroke Localization

Radio-based lightning locating systems estimate source points corresponding to strong dI/dt, which do not necessarily coincide with:

- maxima of the lightning current,
- maxima of dI/dt,
- physical CG attachment points.

This results from uncertainties inherent to Time Difference of Arrival (TDoA) or Direction Finding (DF) methods (Hahn, 1972; Cummins et al., 1998), the frequency response of the receiving antennas, and the fact that all reported stroke locations represent a two-dimensional projection of a three-dimensional discharge process. Furthermore, while a physical lightning stroke is an extended channel segment, lightning location networks operationally reduce this complex structure to a single point-like source location. Throughout this paper, the term "Stroke" therefore refers exclusively to this radio-detected source point reported by the lightning detection network, not to the full spatial extent of the underlying discharge.

Appendix B. Overpass Turbo Queries

Appendix B.1. Wind Turbine Query

```
[out:json][timeout:150];
nwr["generator:source"="wind"] (49, 11, 51, 14);
out center;
```

Appendix B.2. High-Rise Structures Query

```
[out:json][timeout:150];
(
    nwr(if:number(t["height"]) > 70) ["generator:source"!~"wind"]["man_made"](49,
    nwr(if:number(t["building:levels"]) > 25) (49, 11, 51, 14);
);
out center;
```

References

Azadifar, M., Rachidi, F., Rubinstein, M., Paolone, M., Diendorfer, G., Pichler, H., Schulz, W., Pavanello, D., Romero, C., 2016. Evaluation of the performance characteristics of the European Lightning Detection Network EUCLID in the Alps region for upward negative flashes using direct measurements at the instrumented Säntis Tower. Journal of Geophysical Research: Atmospheres 121, 595–606. doi:10.1002/2015JD024259.

Boltek Corporation, 2023. EFM-100 Electric Field Mill — Installation / Operator's Guide (EFM-100C). Accessed: 2024-12-01.

Brook, M., Nakano, M., Krehbiel, P., Takeuti, T., 1982. The electrical structure of the Hokuriku winter thunderstorms. Journal of Geophysical Research: Oceans 87, 1207–1215. doi:10.1029/JC087iC02p01207.

Candela Garolera, A., Madsen, S.F., Nissim, M., Myers, J.D., Holboell, J., 2016. Lightning damage to wind turbine blades from wind farms in the u.s. IEEE Transactions on Power Delivery 31, 1043–1049. doi:10.1109/TPWRD.2014.2370682.

Chen, H., Chen, W., Wang, Y., Xiang, N., He, T., Gu, J., Zhang, S., Sun, T., 2021. Analysis of the cloud-to-ground lightning characteristics before and after installation of the coastal and inland wind farms in china. Electric Power Systems Research 190, 106835. URL: https://www.sciencedirect.com/science/article/pii/S0378779620306350, doi:10.1016/j.epsr.2020.106835.

Cummins, K.L., Murphy, M.J., Bardo, E.A., Hiscox, W.L., Pyle, R.B., Pifer, A.E., 1998. A combined toa/mdf technology upgrade of the u.s. national lightning detection network. Journal of Geophysical Research: Atmospheres 103, 9035–9044. doi:10.1029/98JD00153.

Czech Thunderstorm Research Association, 2019. Vytváří větrné elektrárny bouřky? URL: https://lovcibourek.cz/vytvari-vetrne-elektrarny-bourky/. the article analyzes lightning activity in the vicinity of wind turbines.

Czech Thunderstorm Research Association, 2021. Samostatně iniciované „zimní" blesky. URL: https://lovcibourek.cz/

samostatne-iniciovane-zimni-blesky/. the article describes the phenomenon of self-initiated lightning. The article has an operational character and summarizes ongoing results of the OROSTREP project.

Eriksson, A.J., 1987. The incidence of lightning strikes to power lines. IEEE Transactions on Power Delivery 2, 859–870. doi:10.1109/TPWRD.1987.4308191.

Grosshans, H., Szász, R.Z., Papalexandris, M.V., 2017. Modeling the electrostatic charging of a helicopter during hovering in dusty atmosphere. Aerospace Science and Technology 64, 31–38. doi:10.1016/j.ast.2016.12.032.

Hahn, S.L., 1972. A new approach to hyperbolic navigation. IEEE Transactions on Aerospace and Electronic Systems AES-8, 260–268. doi:10.1109/TAES.1972.309614.

Haklay, M., 2010. How good is volunteered geographical information? a comparative study of openstreetmap and ordnance survey datasets. Environment and Planning B: Planning and Design 37, 682–703. URL: https://doi.org/10.1068/b35097, doi:10.1068/b35097, arXiv:https://doi.org/10.1068/b35097.

Heidler, F., Zischank, W., Manhardt, M., 2013. The slow-varying electric field of negative upward lightning initiated by the Peissenberg Tower, Germany. IEEE Transactions on Electromagnetic Compatibility 55, 353–361. doi:10.1109/TEMC.2012.2209121.

Hersbach, H., Bell, B., Berrisford, P., et al., 2020. The ERA5 global reanalysis. Quarterly Journal of the Royal Meteorological Society 146, 1999–2049. doi:10.1002/qj.3803.

Kákona, J., Mikeš, J., Ambrožová, I., Ploc, O., Velychko, O., Sihver, L., Kákona, M., 2023. In situ ground-based mobile measurement of lightning events above central europe. Atmospheric Measurement Techniques 16, 547–561. doi:10.5194/amt-16-547-2023.

Matsui, M., Michishita, K., Yokoyama, S., 2020. Cloud-to-ground lightning flash density and the number of lightning flashes hitting wind turbines in japan. Electric Power Systems Research 181,

106066. URL: https://www.sciencedirect.com/science/article/pii/S0378779619303852, doi:10.1016/j.epsr.2019.106066.

Montanyà, J., Fabró, F., van der Velde, O., et al., 2016. Global distribution of winter lightning: a threat to wind turbines and aircraft. Natural Hazards and Earth System Sciences 16, 1465–1472. doi:10.5194/nhess-16-1465-2016.

Montanyà, J., van der Velde, O., Williams, E.R., 2014. Lightning discharges produced by wind turbines. Journal of Geophysical Research: Atmospheres 119, 1455–1462. URL: https://agupubs.onlinelibrary.wiley.com/doi/abs/10.1002/2013JD020225, doi:10.1002/2013JD020225, arXiv:https://agupubs.onlinelibrary.wiley.com/doi/pdf/10.1002/2013JD020225.

Morgenstern, D., Stucke, I., Simon, T., Mayr, G.J., Zeileis, A., 2022. Differentiating lightning in winter and summer with characteristics of the wind field and mass field. Weather and Climate Dynamics 3, 361–375. doi:10.5194/wcd-3-361-2022.

Narita, T., Wanke, E., Sato, M., Sakanoi, T., Kumada, A., Kamogawa, M., Ishikawa, H., Harada, S., Kameda, T., Tsuchiya, F., Kaneko, E., 2018. A study of lightning location system (blitz) based on vlf sferics, in: 2018 34th International Conference on Lightning Protection (ICLP), IEEE. pp. 1–7. doi:10.1109/ICLP.2018.8503311.

OpenStreetMap contributors, 2024. Planet dump retrieved from https://planet.osm.org. https://www.openstreetmap.org. Accessed: 2025-01-01.

Overpass API Developers, 2025. Overpass turbo. URL: https://overpass-turbo.eu. accessed: 2025-01.

Rakov, V.A., 2003. A review of the interaction of lightning with tall objects. Recent Research Developments in Geophysics 5, 57–71.

Rakov, V.A., Uman, M.A., 2003. Lightning: Physics and Effects. Cambridge University Press, Cambridge, UK. doi:10.1256/wea.168/03.

Saunders, C.P.R., Bax-norman, H., Emersic, C., Avila, E.E., Castellano, N.E., 2006. Laboratory studies of the effect of cloud conditions on graupel/crystal charge transfer in thunderstorm elec-

trification. Quarterly Journal of the Royal Meteorological Society 132, 2653–2673. URL: https://rmets.onlinelibrary.wiley.com/doi/abs/10.1256/qj.05.218, doi:10.1256/qj.05.218, arXiv:https://rmets.onlinelibrary.wiley.com/doi/pdf/10.1256/qj.05.218.

Smorgonskiy, A., Rachidi, F., Rubinstein, M., Diendorfer, G., Schulz, W., 2013. On the proportion of upward flashes to lightning research towers. Atmospheric Research 129–130, 110–116. doi:10.1016/j.atmosres.2012.09.008.

Smorgonskiy, A., Tajalli, A., Rachidi, F., Rubinstein, M., Diendorfer, G., Pichler, H., 2015. An analysis of the initiation of upward flashes from tall towers with particular reference to Gaisberg and Säntis Towers. Journal of Atmospheric and Solar-Terrestrial Physics 136, 46–51. doi:10.1016/j.jastp.2015.06.016.

Soula, S., Georgis, J.F., Salaün, D., 2019. Quantifying the effect of wind turbines on lightning location and characteristics. Atmospheric Research 221, 98–110. doi:10.1016/j.atmosres.2019.01.010.

Stucke, I., Morgenstern, D., Zeileis, A., Mayr, G.J., Simon, T., Diendorfer, G., Schulz, W., Pichler, H., 2024. Diagnosing upward lightning from tall objects from meteorological thunderstorm environments. Electric Power Systems Research 229, 110199. doi:10.1016/j.epsr.2024.110199.

Takahashi, T., 1978. Riming electrification as a charge generation mechanism in thunderstorms. Journal of the Atmospheric Sciences 35, 1536–1548. doi:10.1175/1520-0469(1978)035<1536:REAACG>2.0.CO;2.

Takahashi, T., Tajiri, T., Sonoi, Y., 1999. Charges on graupel and snow crystals and the electrical structure of winter thunderstorms. Journal of the Atmospheric Sciences 56, 1561–1578. doi:10.1175/1520-0469(1999)056<1561:COGASC>2.0.CO;2.

Vaisala, 2024. Vaisala Weather Radar Software: Hydrometeor Classification (HClass). Vaisala Oyj. Helsinki, Finland. URL: https://www.vaisala.com/en/products/vaisala-weather-radars.

Wanke, E., 2011. Blitzortung.org – a low-cost time of arrival lightning detection and location network (green pcb 6.6 / pcb 5.6 documentation). https://www.blitzortung.org/Compendium/Documentations/

Documentation_2011-04-01_Green_PCB_6.6_PCB_5.6.pdf. Accessed: 2025-12-01.

Zhu, Y., Rakov, V.A., Tran, M.D., Stock, M.G., Heckman, S., Liu, C., Sloop, C.D., Jordan, D.M., Uman, M.A., Caicedo, J.A., Kotovsky, D.A., Wilkes, R.A., Carvalho, F.L., Ngin, T., Gamerota, W.R., Pilkey, J.T., Hare, B.M., 2017. Evaluation of entln performance characteristics based on the ground truth natural and rocket-triggered lightning data acquired in florida. Journal of Geophysical Research: Atmospheres 122, 9858–9866. URL: https://agupubs.onlinelibrary.wiley.com/doi/abs/10.1002/2017JD027270, doi:https://doi.org/10.1002/2017JD027270, arXiv:https://agupubs.onlinelibrary.wiley.com/doi/pdf/10.1002/2017JD027270.

Zhu, Y., Stock, M., Lapierre, J., DiGangi, E., 2022. Upgrades of the Earth Networks Total Lightning Network in 2021. Remote Sensing 14, 2209. URL: https://doi.org/10.3390/rs14092209, doi:10.3390/rs14092209.